Human Molecular Genetics, 2004, Vol. 13, No. 16 ***1727–1743***
doi:10.1093/hmg/ddh185
Advance Access published on June 15, 2004

Evidence for a dominant-negative effect in *ACTA1* nemaline myopathy caused by abnormal folding, aggregation and altered polymerization of mutant actin isoforms

Biljana Ilkovski[1,2], Kristen J. Nowak[3,4], Ana Domazetovska[1,2], Adam L. Maxwell[1], Sophie Clement[5], Kay E. Davies[4], Nigel G. Laing[3], Kathryn N. North[1,2] and Sandra T. Cooper[1,*]

[1]The Institute for Neuromuscular Research, The Children's Hospital at Westmead, [2]Discipline of Paediatrics and Child Health, Faculty of Medicine, University of Sydney, Australia, [3]Centre for Neuromuscular and Neurological Disorders, University of Western Australia (UWA); Australian Neuromuscular Research Institute and Centre for Medical Research, UWA; West Australian Institute for Medical Research, Queen Elizabeth II Medical Centre, Nedlands, Western Australia, [4]MRC Functional Genetics Unit, Department of Human Anatomy and Genetics, University of Oxford, UK and [5]Department of Pathology, University of Geneva, Geneva, Switzerland

Received March 31, 2004; Revised and Accepted June 3, 2004

We have studied a cohort of nemaline myopathy (NM) patients with mutations in the muscle α-skeletal actin gene (*ACTA1*). Immunoblot analysis of patient muscle demonstrates increased γ-filamin, myotilin, desmin and α-actinin in many NM patients, consistent with accumulation of Z line-derived nemaline bodies. We demonstrate that nebulin can appear abnormal secondary to a primary defect in actin, and show by isoelectric focusing that mutant actin isoforms are present within insoluble actin filaments isolated from muscle from two *ACTA1* NM patients. Transfection of C2C12 myoblasts with mutant actin$_{EGFP}$ constructs resulted in abnormal cytoplasmic and intranuclear actin aggregates. Intranuclear aggregates were observed with V163L–, V163M– and R183G–actin$_{EGFP}$ constructs, and modeling shows these residues to be adjacent to the nuclear export signal of actin. V163L and V163M actin mutants are known to cause intranuclear rod myopathy, however, intranuclear bodies were not reported in patient R183G. Transfection studies in C2C12 myoblasts showed significant alterations in the ability of V136L and R183G actin mutants to polymerize and contribute to insoluble actin filaments. Thus, we provide direct evidence for a dominant-negative effect of mutant actin in NM. *In vitro* studies suggest that abnormal folding, altered polymerization and aggregation of mutant actin isoforms are common properties of NM *ACTA1* mutants. Some of these effects are mutation-specific, and likely result in variations in the severity of muscle weakness seen in individual patients. A combination of these effects contributes to the common pathological hallmarks of NM, namely intranuclear and cytoplasmic rod formation, accumulation of thin filaments and myofibrillar disorganization.

INTRODUCTION

Nemaline myopathy (NM) is an inherited muscle disorder characterized by muscle weakness and the presence of rod bodies within the muscle fibers of affected patients. Clinically, presentation of NM ranges from severe-congenital (lethal), to milder childhood- or adult-onset forms. NM is genetically heterogenous, with disease-causing mutations identified in genes encoding five different components of the thin filament. Linkage analysis suggests that nebulin (*NEB*) may be the most common cause of NM (1). However, the nebulin gene is large and highly repetitive and thus difficult to screen for mutations. Consequently, nebulin mutations have been identified in only a moderate number of patients to date (2–4). Mutations in α-skeletal actin are the second most common cause of NM, accounting for ∼20% of cases (5–7). Rare mutations have

*To whom correspondence should be addressed at: Institute for Neuromuscular Research, The Children's Hospital at Westmead, Locked Bag 4001, Westmead, NSW 2145, Australia. Tel: +61 298451220; Fax: +61 298453078; Email: sandrac3@chw.edu.au

also been identified in α-tropomyosin$_{slow}$ (*TPM3*) (8–10), β-tropomyosin (*TPM2*) (11) and troponin T1 (*TNNT1*) (12).

To date, 91 *ACTA1* mutations have been identified, and are distributed throughout the entire actin gene (6) (N.G. Laing, unpublished data). Mutations in *ACTA1* cause at least three distinct pathological phenotypes: (1) cytoplasmic nemaline bodies; (2) large myoplasmic accumulations of filamentous actin; and (3) intranuclear rods.

The majority of actin NM cases result from dominant *de novo* mutations. However, several families with autosomal dominant actin NM (5,6,13), and rare cases of autosomal recessive NM with compound heterozygous skeletal actin mutations have also been described (6). A severe-lethal NM patient homozygous for an actin nonsense mutation (R39X) has also been identified (6,14). The patient was born to consanguineous parents who were shown to be heterozygous for the actin null mutation (N.G. Laing *et al.*, unpublished data). These results indicate that haploinsufficiency of actin does not underlie NM. This is supported by transgenic mouse studies, which demonstrate the heterozygote *ACTA1* +/− mice have a normal lifespan and no evidence of muscle weakness, whereas homozygous *ACTA1* knock-out mice do not express any α-skeletal actin and die from muscle weakness and starvation within 9 days after birth (15). Similarly, homozygous expression of a null mutation within the sarcomeric actin isoform (*Act88F*) of *Drosophila* indirect flight muscle results in a flightless phenotype and severe sarcomeric abnormalities (16,17).

The fact that mutant actin isoforms produce dominant-negative effects in yeast (18) and *Drosophila* (17,19), suggests that a dominant-negative mode of disease pathogenesis is likely in many NM patients with *ACTA1* mutations. NM actin mutations are likely to differentially affect specific actin-binding interactions, and they may also invoke distinct structural changes within the actin molecule or filament (6). Nevertheless, multiple different actin mutations all result in the same pathology of muscle weakness and nemaline rod formation.

We have shown previously the abnormal localization of other thin-filament proteins, such as tropomyosin and nebulin, in patients with characterized *ACTA1* mutations (5). Therefore, this study sought to extend these observations and examine the expression of a large panel of sarcomeric and thin-filament proteins in our cohort of actin NM patients. We sought to confirm the presence of mutant actin isoforms within the sarcomeric and cytoskeletal actin filaments, through isoelectric focusing, to confirm a dominant-negative mode of disease pathogenesis. Furthermore, we have used transfection studies in cultured myoblasts and myotubes to examine abnormal aggregation of mutant actin isoforms, and to demonstrate alterations in the equilibrium between filamentous and soluble actin forms.

RESULTS

This study examines a series of 10 NM patients with mutations in *ACTA1* (Table 1). Patient T66I and patient E72K are two new patients with *ACTA1* mutations not previously described. Patient T66I was born at term with severe hypotonia and minimal spontaneous movements of the arms and legs. Although she could breathe independently, she had difficulty with secretions and required a gastronomy tube for feeding. The patient died of respiratory failure at 4.5 months of age. Gomori trichrome preparation of the patient's muscle biopsy shows numerous nemaline bodies within most muscle fibers (Fig. 1A), but muscle of good overall histology, with normal, well-packed fascicular bundles of muscle fibers. Electron microscopy (EM) reveals nemaline bodies (Fig. 1B) and accumulations of amorphous material (Fig. 1C, arrowhead). The patient was found to have a *de novo* missense mutation within *ACTA1* not observed in either parent, resulting in an amino acid substitution of T66I (ACC → ATC).

Patient E72K is heterozygous for a *de novo ACTA1* E72K substitution (GAG → AAG). She was born at 35 weeks gestation with severe arthrogryposis and multiple contractures and fractures. She had a high arched palate, pectus excavatum, poor muscle development of the limbs, and died 2 h after birth from respiratory failure. The autopsy report was unremarkable except for analysis of the quadriceps muscle, which contained numerous nemaline bodies, moderate variation in fibre size and predominance of very small fibers. Examination of sections of the psoas and the diaphragm showed myopathic changes but did not show nemaline bodies. Gomori trichrome preparation of autopsy samples from the patient's quadriceps muscle shows numerous nemaline bodies within most muscle fibers, poor packing of muscle fibers and severely atrophied rod-containing fibers (Fig. 1D). EM revealed severe sarcomeric disorganization and the presence of nemaline bodies (Fig. 1E). EM analysis also revealed cytoplasmic bodies (long arrowhead) and glycogen accumulations (short arrowhead) (Fig. 1F).

Patient V163M has been briefly reported (6) and is described here in more detail. She presented in the neonatal period with severe weakness, and at 8 months of age required nasogastric feeding due to difficulties with swallowing. At 3.5 years of age she was able to walk and swallow. Her mother and grandfather had more mild facial and limb muscle weakness, and also carry the V163M mutation. Gomori trichrome staining of her muscle biopsy reveals numerous intranuclear (IN) rods (Fig. 1G, arrowheads). EM analysis defines more clearly the crystalline intranuclear inclusions (Fig. 1H), and also reveals muscle fibers with regions of amorphous material (Fig. 1I, long arrow) and filamentous accumulations (Fig. 1I, short arrow and inset). Similar IN rods and filamentous accumulations were observed in the grandfather. However, filamentous accumulations, but not IN rods, were evident in the biopsy specimen obtained from the mother (data not shown). The absence of detectable IN rods in the mother may reflect sampling, a gene dosage effect, or variation in IN rod formation between different muscles.

Immunostaining of muscle biopsy (rectus abdominus) samples from patient T66I shows normal staining for actin, nebulin and tropomyosin (Fig. 2D–F). Despite the extreme myofibrillar disorganization within the muscle of patient E72K, tropomyosin was present in all visible fibers, and exhibited striated staining (Fig. 2I). In addition, α-actinin 2 positively labeled all fibers, and there was normal labeling for myosin heavy-chain isoforms (slow, fast and developmental), and members of the dystrophin complex (dystrophin,

Table 1. Summary of *ACTA1* nemaline myopathy patients

	ACTA1 mutation	NM classification	Phenotype of actin–GFP fusion proteins in C2C12
1	T66I	Severe congenital	Similar to WT–$actin_{EGFP}$
2	E72K	Severe congenital	Similar to WT–$actin_{EGFP}$
3	$N115S_a$ (13,5)	Childhood onset	Similar to WT–$actin_{EGFP}$
4	$N115S_b$ (13,5)	Typical congenital	
5	I136M (5)	Typical congenital	Cytoplasmic aggregates only
6	V163L (33)	Severe congenital Typical congenital	Predominantly intranuclear aggregates Some cytoplasmic aggregates
7	V163M (6)	Typical congenital	Predominantly intranuclear aggregates Some cytoplasmic aggregates
8	R183G (5)	Severe congenital	Intranuclear and cytoplasmic aggregates Actin filament fragmentation
9	G268C (5)	Childhood onset	Similar to wild-type $actin_{EGFP}$
10	I357L (5)	Severe congenital	Similar to wild-type $actin_{EGFP}$

sarcoglycans and laminin α2) (data not shown). In contrast, immunostaining for actin and nebulin demonstrated marked abnormalities (Fig. 2G and H). Nebulin immunostaining was performed using five different nebulin antibodies, all of which showed very abnormal staining, with many negative fibers (Fig. 2H). Consequently, a defect in the nebulin gene was also considered as a potential disease candidate in this patient. The identification of a primary abnormality within *ACTA1* emphasizes that nebulin can appear abnormal secondarily to a primary defect in actin, a finding mirrored in previous studies (5). Thus, nebulin abnormalities may be a pathological consequence of primary actin mutations that result in severe disruption of the sarcomeric thin filament, and patients should be screened for mutations in *ACTA1* before pursuit of nebulin as the disease candidate.

A mutation in α-skeletal actin affects expression of other thin-filament proteins

We have characterized the expression of a panel of sarcomeric and thin-filament proteins in eight NM patients with characterized mutations in α-skeletal actin (Fig. 3). For comparison, we have also shown data from a NM patient with a mutation in α-$tropomyosin_{slow}$ (*TPM3*, M9R) (Fig. 3A, lanes 7 and 8). Muscle biopsy samples were separated into insoluble and soluble protein pools using a buffer containing 0.5% Triton X-100. Although separation of soluble versus insoluble protein pools by this method is relatively crude, the insoluble fraction represents proteins within the insoluble cytoskeleton and sarcomeric apparatus. This fraction may also contain proteins present within nemaline bodies. The soluble fraction contains soluble proteins, or short filaments not sedimented by centrifugation at 15 000*g*.

Solubilized muscle samples normalized for myosin content were separated by gradient sodium dodecyl sulfate–polyacrylamide gel electrophoresis (SDS–PAGE), and PVDF membranes were sectioned and probed with multiple antibodies. Figure 3A represents data from patients with mild NM with typical congenital- or childhood-onset forms of the disorder (aged 5–46 years, see figure legends for details). Figure 3B represents data from patients with severe congenital NM, all of whom died within the first year of life (neonatal samples). It is important to emphasize that these studies represent analysis of a single biopsy specimen from affected patients, and in one case the experiment could be repeated only once (patient I357L), because of the scarcity of the biopsy specimen available. Nevertheless, several trends were observed. We detected a general increase in levels of γ-filamin, α-actinin, myotilin and desmin in many NM patients, compared with unaffected age-matched controls (Fig. 3A and B). These proteins are known to associate with the Z-disc of muscle (20–25), thus elevated levels of these proteins would be consistent with accumulation of Z line-derived nemaline bodies within NM patient samples.

An additional tropomyosin band migrating above β-tropomyosin was observed in patient G268C, and in the adductor pollicis (TPM_a), but not in the deltoid muscle (TPM_b) of the *TPM3* (M9R) NM patient. This band likely corresponds to expression of another high molecular weight tropomyosin isoform. The TM311 antibody used in this study recognizes exon 1a of the *TPM1* (alpha fast), *TPM2* (beta) and *TPM3* (alpha slow) tropomyosin genes (26) contained in all sarcomeric tropomyosins. However, exon 1a is also expressed in smooth muscle (27) and fibroblast (28) high molecular weight tropomyosin isoforms (reviewed in 29). Patient TPM has a primary mutation in α-$tropomyosin_{slow}$ (M9R), and exhibits an altered ratio of α- and β-tropomyosin isoforms, with increased levels of α-$tropomyosin_{slow}$ and reduced levels of β-tropomyosin (30).

Higher levels of troponin I_{slow} are seen in the soluble fraction of NM muscle, relative to controls, and expression of troponin I_{fast} closely parallels the fibre-type distribution observed in these NM patients. Patients G268C, I136M, $N115S_a$, $N115S_b$ and TPM M9R have almost complete Type 1 fibre predominance (5 and unpublished data) and a virtual absence of immunoreactivity for troponin I_{fast} (Fig. 3A). In contrast, patients R183G and NM2 both possess 50% of fibers that stain positively for fast myosin, and are also shown to express significant levels of troponin I_{fast} by western analysis (Fig. 3B, lanes 5 and 6). For patient T66I, the biopsy specimen taken at birth (39 weeks, vastus lateralis) has 80% fast (and neonatal) myosin positive fibers (data not shown) and also shows expression of troponin I_{fast} (Fig. 3B, lane 3). In contrast, the biopsy specimen taken at 10 weeks (rectus abdominus) displays virtually complete Type 1 fibre predominance (data not shown), with

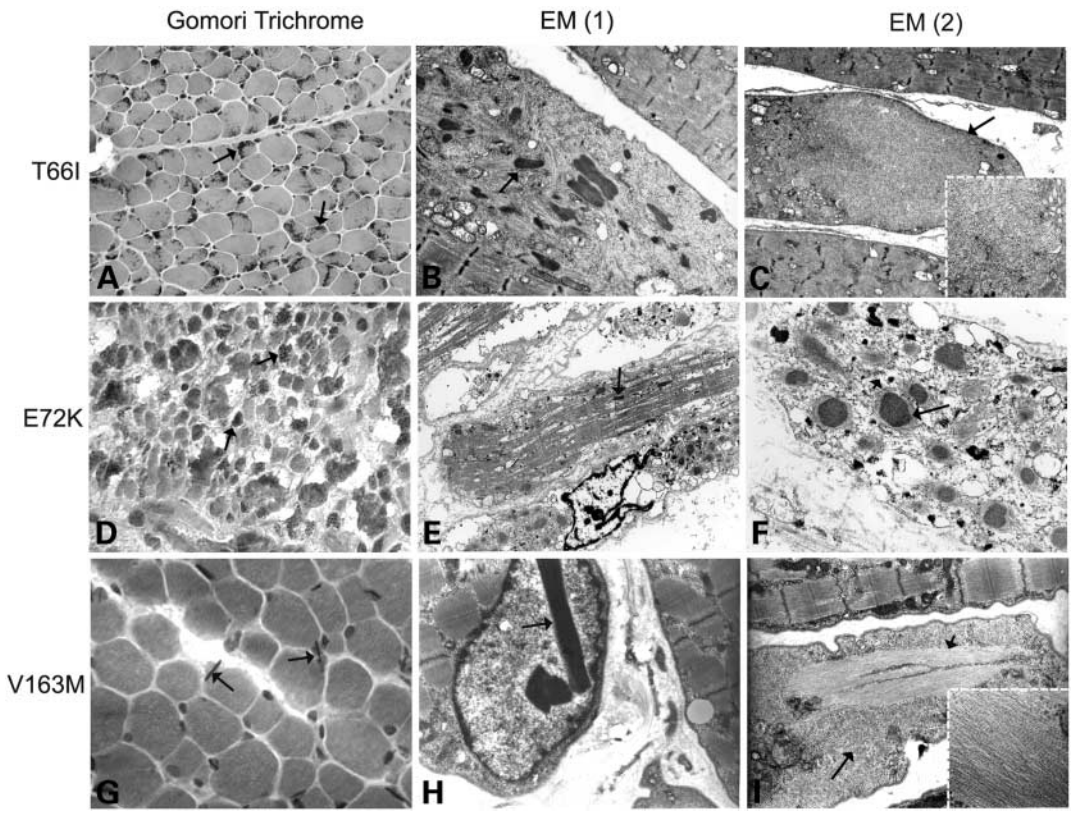

Figure 1. Muscle histology in *ACTA1* nemaline myopathy patients T66I, E72K and V163M. Gomori trichrome staining of frozen muscle sections shows cytoplasmic nemaline bodies in patients T66I [(**A**) rectus abdominus, 400× magnification] and E72K [(**D**) quadriceps, 1000×], and intranuclear rods in patient V163M [(**G**) 1000×] (arrows). Electron microcopy (EM) confirms the presence of nemaline bodies (arrowheads) in all three patients [(**B**) 25 000×; (**E**) 730×; (**H**) magnification unavailable]. Accumulations of amorphous material (long arrows), devoid of sarcomeric register and organelles, were evident in muscle fibers from patients T66I [**C**) 5000× and inset 17 000×] and V163M [(**I**) magnification unavailable]. Accumulations of filamentous material were a common feature in patient V163M, particularly in subsarcolemmal regions. (I) shows filamentous accumulations (short arrow) within a large region of amorphous material. A higher magnification image shows long filaments with partial striations [(I) inset, magnification unavailable]. Cytoplasmic bodies [(**F**) long arrow] and glycogen accumulations [(**F**) short arrow] were a common feature in muscle from patient E72K.

no evidence for expression of troponin I_{fast} (Fig. 3B, lane 4). Although it is tantalizing to infer that these findings may reflect slow fibre conversion during the early postnatal period for patient T66I, a direct comparison is not without ambiguity, given the two biopsy samples are derived from distinct sites.

Higher levels of cardiac actin were observed in several severely affected NM neonates, compared with age-match controls (Fig. 3B; compare patient samples in lanes 2–4 and 9, with age-matched controls in lanes 1 and 7). Cardiac actin is expressed in human skeletal muscle during development, and is down-regulated in the early postnatal period (data not shown). Elevated levels of cardiac actin have also been observed by immunostaining in severely affected NM neonates (5 and data not shown), and may reflect altered maturation or fibre regeneration in these patients. Immunoblot analysis for α-skeletal actin shows broadly similar levels of expression in both NM patients and controls, with the exception of the NM disease control (Fig. 3B, lane 2, NM1), for whom an *ACTA1* mutation has been excluded, using the standard *ACTA1* mutation screen (5). Low levels of skeletal actin relative to higher levels of cardiac actin were observed in this patient (NM1). Multiple bands for α-skeletal actin were observed in several severe lethal NM patients, and may reflect increased degradation of actin in muscle of severely affected patients.

Western analysis for nebulin is challenging, owing to its extremely large size and insolubility. We observed variation in levels of nebulin expression in control samples, despite using an antibody recognizing the extreme N-terminus of nebulin that is thought to be present in all isoforms (31). Despite this variability, very low levels or absent nebulin was observed in several NM patients. The very low or absent nebulin signal persisted even with long exposures, was evident in repeat experiments, and exceeded the normal variation observed with control samples. In addition, nebulin immunoreactivity was seen in the base of two wells loaded with samples derived from two severely affected NM patients [Fig. 3B, lanes 2 (NM1) and 10 (I357L)]. This pool of insoluble or poorly solubilized nebulin may reflect the diseased state of these muscle samples, which contained extremely high levels of nemaline bodies within the muscle fibers.

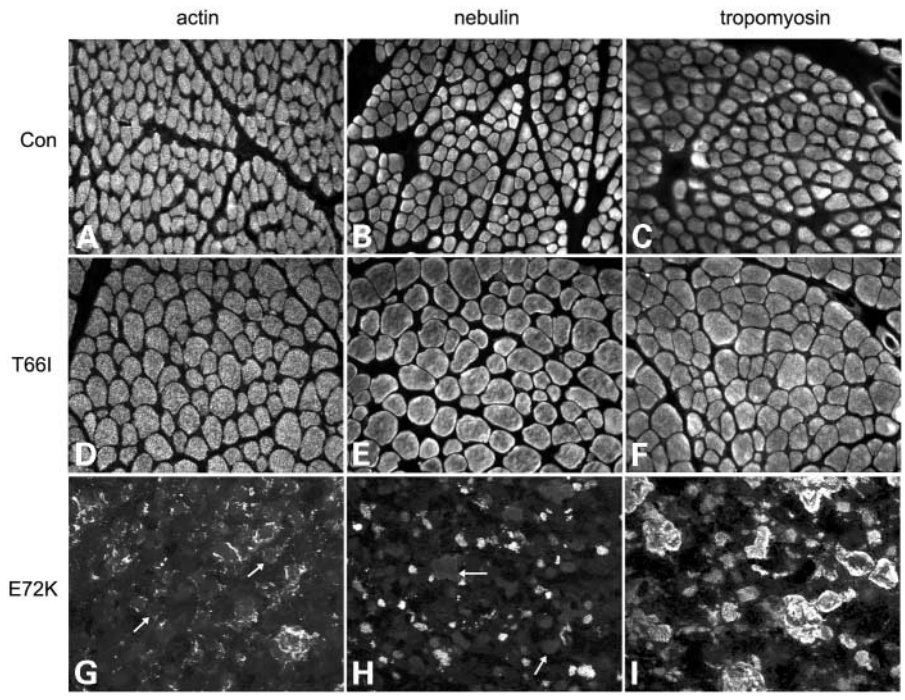

Figure 2. Nebulin immunostaining may be abnormal in NM patients with a primary actin mutation. Immunohistochemical analysis of frozen muscle biopsy sections from severe *ACTA1* NM patients T66I and E27K, and an age-matched control. Muscle cryosections (8 μm) were stained with antibodies recognizing sarcomeric actin (mAb 5C5, Sigma, recognizes α-skeletal and α-cardiac actin), nebulin (NB2) and sarcomeric tropomyosin (TM311), followed by a CY3-conjugated secondary antibody. Actin, nebulin and tropomyosin showed normal homogenous labeling in control [(**A**–**C**) 400×] and patient T66I [(**D**–**F**, 400×] muscle fibers. Despite the extreme diseased state of the muscle from patient E72K [(**G**–**I**) 1000×], staining for (G) actin and (H) nebulin was markedly abnormal, with many negative fibers (arrows), whereas tropomyosin staining was detected in all visible fibers (I). Images were captured using an Olympus BX50 microscope linked to a SPOT™ digital imaging camera (Diagnostic Instruments Inc.) with Advanced V3.0.4 software, using 40× (UPlanFl 0.75) and 100× (UPlanFl 1.30 oil) lenses.

IEF shows mutant actin isoforms R183G and E72K are expressed at significant levels within muscle actin filaments

Missense mutations resulting in amino acid charge changes in two of our severe actin NM patients were exploited to examine levels of mutant and wild-type (WT) actin within muscle biopsy specimens through isoelectric focusing (IEF) (Fig. 4). In whole muscle lysates of control muscle, a major single spot corresponding to wild-type α-skeletal actin (predicted p*I* of 5.23) is observed (Fig. 4A, WT). In contrast, two spots are clearly evident for patients R183G and E72K. The R183G mutant actin (predicted p*I* of 5.16) is more acidic, and appears to be expressed at roughly equal levels to wild-type actin (R183G, arrowhead). In contrast, actin-E72K is more basic (predicted p*I* of 5.38) and appears to be present at slightly reduced levels (E72K, arrowhead), compared with wild-type actin.

To further explore the hypothesis of a dominant-negative effect of mutant actin in NM, we sought to determine whether mutant actin isoforms were correctly targeted to the insoluble pool (the cytoskeletal and sarcomeric apparatus), or were instead localized within the soluble protein fraction (actin monomers and short actin filaments). Muscle samples were extracted with 0.5% Triton X-100 buffer to separate soluble and insoluble fractions. Proteins contained in each fraction were denatured in IEF rehydration solution containing 8 M urea, 2% Triton X-100 and 36 mM dithiothreitol (DTT). Relative levels of α-skeletal actin in each fraction were first determined through western blot, so appropriate amounts of each sample could be loaded onto IEF strips for analysis. IEF analysis of soluble and insoluble protein (adjusted for α-skeletal actin content) show a single spot for control muscle, and two spots in both the insoluble and soluble protein pools in patients R183G and E72K (Fig. 4B). Our results demonstrate that mutant actin isoforms R183G and E72K are expressed at significant levels within the pool of insoluble actin filaments in these two patients. These studies utilize an antibody that specifically recognizes alpha-skeletal actin (32), which predominantly exists as sarcomeric actin comprising the thin filament. Therefore, our results suggest that the mutant actin isoforms are incorporated into sarcomeric thin filaments, supporting the hypothesis that disease pathogenesis in NM patients R183G and E72K results from a dominant-negative (poison-protein) effect, rather than a shortage of normal actin protein. However, the mutant actin isoform may also be contained within cytoskeletal actin filaments or nemaline bodies that do not comprise the sarcomeric thin filament.

α-Skeletal actin mutants form abnormal aggregates in transfected C2C12 myoblasts

To examine the localization of mutant actin isoforms within the actin cytoskeleton of C2C12 myoblasts, C-terminal tagged actin–enhanced green fluorescent protein (EGFP)

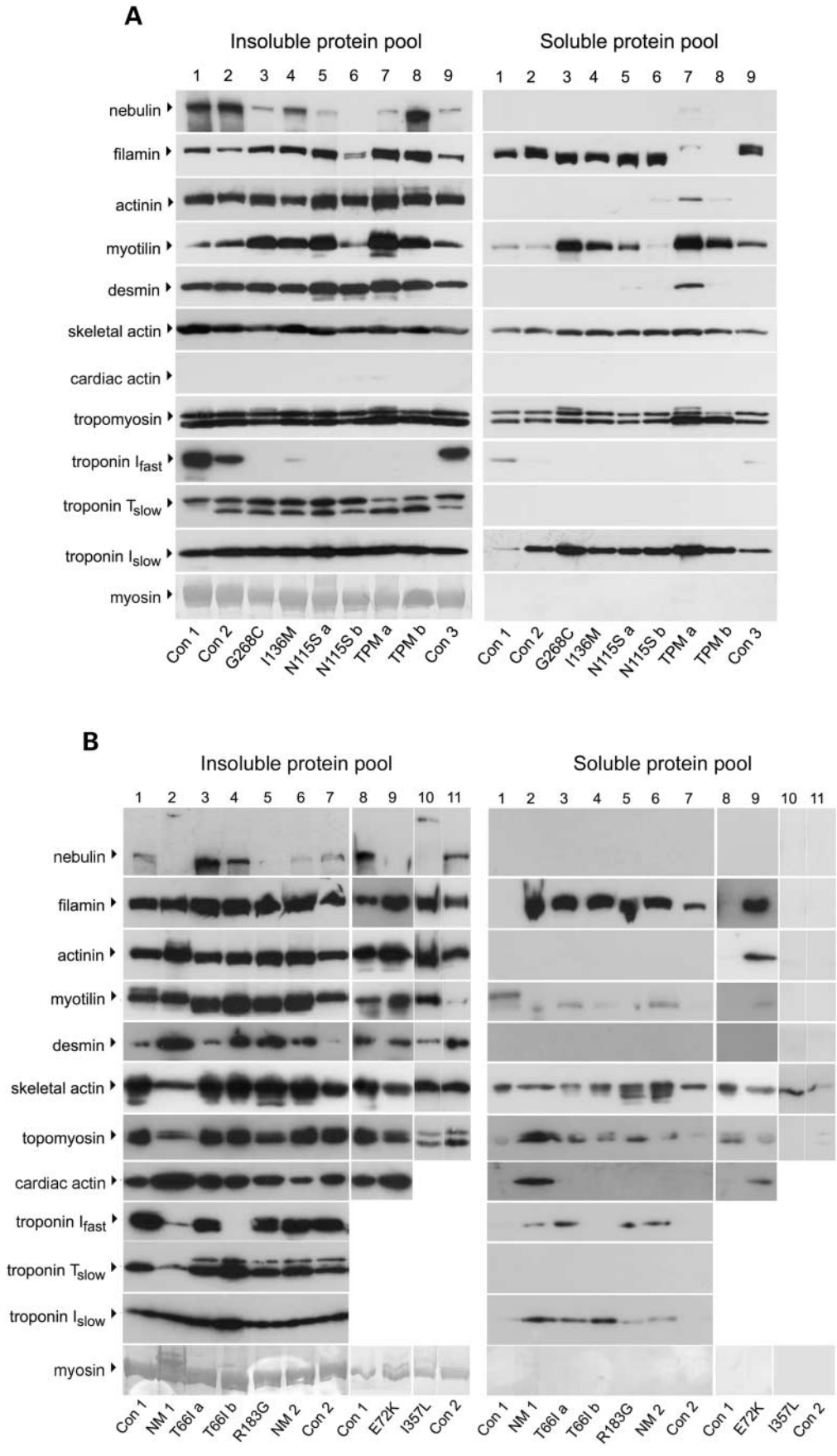
A
Insoluble protein pool
Soluble protein pool
1 2 3 4 5 6 7 8 9
nebulin
filamin
actinin
myotilin
desmin
skeletal actin
cardiac actin
tropomyosin
troponin I fast
troponin T slow
troponin I slow
myosin
Con 1
Con 2
G268C
I136M
N115S a
N115S b
TPM a
TPM b
Con 3
B
Insoluble protein pool
Soluble protein pool
1 2 3 4 5 6 7 8 9 10 11
nebulin
filamin
actinin
myotilin
desmin
skeletal actin
topomyosin
cardiac actin
troponin I fast
troponin T slow
troponin I slow
myosin
Con 1
NM 1
T66I a
T66I b
R183G
NM 2
Con 2
E72K
I357L

fusion constructs were generated. Transfections with wild-type actin–EGFP (WT-actin$_{EGFP}$) into C2C12 myoblasts typically produced stress-fibre or diffuse cytoplasmic staining (Fig. 5A). In contrast, transfection of C2C12 myoblasts with several mutant actin–EGFP constructs produced brightly fluorescent actin–EGFP accumulations located within the cytoplasm and nucleus of transfected cells (Fig. 5A). A summary of actin aggregates formed by different mutant actin$_{EGFP}$ constructs is presented in Table 1.

Intranuclear actin aggregates were a striking feature of V163L–actin$_{EGFP}$ and V163M–actin$_{EGFP}$ transfected C2C12 myoblasts (Fig. 5A, V163L, V163M), although cytoplasmic aggregates were also observed in a subset of transfected cells (data not shown). Only very low levels of cytoplasmic or stress-fibre staining for transfected V163L–actin$_{EGFP}$ and V163M–actin$_{EGFP}$ were detected. Intranuclear aggregates were observed as either brightly fluorescent 'oblong rods' (Fig. 5A), or 'star-like' intranuclear bodies (Fig. 5B,i). The V163L and V163M mutations have been identified in patients with intranuclear rod myopathy, a phenotype which seems to result specifically, but not exclusively, from mutation of residue V163 (6,33,34). The oblong intranuclear aggregates formed by V163L–actin$_{EGFP}$ and V163M–actin$_{EGFP}$ constructs in C2C12 myoblasts closely resemble intranuclear bodies observed in muscle samples from patients with intranuclear myopathy (Fig. 1G).

In this study, intranuclear actin accumulations were also observed with a third construct, R183G–actin$_{EGFP}$ (Fig. 5A, R183G). However, the R183G mutation was found in a severe lethal NM patient (5) whose muscle biopsy did not show intranuclear rods. Unlike V163L and V163M actin mutants, significant levels of diffuse cytoplasmic staining, with occasional labeling of stress fibers, were observed in R183G–actin$_{EGFP}$-transfected cells (Fig. 5A). Fragmentation of actin filaments, and large aggregates of cytoplasmic actin were also features of a subset of actin–R183G$_{EGFP}$ transfected cells (Fig. 5B,ii). Molecular modeling shows that amino acid residues V163 and R183 are adjacent to the actin nuclear export signal (NES) (35), lying within the 4 Å maximal radius for bond formation (Fig. 8B). Therefore, V163L, V163M and R183G actin mutations may affect the conformation or binding properties of the NES, resulting in retention and aggregation of these actin isoforms within the nucleus (see Discussion).

The I136M–actin$_{EGFP}$ construct produced exclusively cytoplasmic accumulations, in only a subset of transfected cells. The cytoplasmic localization of I136M–actin$_{EGFP}$ aggregates is consistent with the pathology of patient I136M, which shows only cytoplasmic nemaline bodies. I136M–actin$_{EGFP}$ actin aggregates had a distinct morphology, typical of 'a line drawn by a highlighter pen' (Fig. 5B,iii). Occasionally, I136M–actin$_{EGFP}$ accumulations would also be 'kinked' (Fig. 5B,iii, inset). Transfection studies with several mutant actin$_{EGFP}$ constructs (G268C, N115S, I357L, E72K, T66I) did not produce actin aggregates, but resulted in normal stress-fibre or diffuse cytoplasmic staining, similar to WT–actin$_{EGFP}$ (data not shown). Very infrequently, rod-shaped aggregates could be observed in one or two cells from coverslips transfected with WT-actin, and pathologically unremarkable mutant actin constructs. Although rarely observed, aggregation of WT–actin$_{EGFP}$ may represent a normal response of cells to inappropriate folding or processing of actin, that is exacerbated with particular actin mutations.

Phalloidin labeled the majority of mutant actin$_{EGFP}$ aggregates (Fig. 5A, phalloidin), with the exception of I136M–actin$_{EGFP}$, for which no phalloidin labeling could be observed (Fig. 5B, iv). I136M–actin$_{EGFP}$ aggregates also did not label with DNase I (data not shown). Thus, I136M–actin$_{EGFP}$ aggregates may indeed constitute filamentous actin, but exhibit a tertiary conformation that is incompatible with phalloidin binding. Alternately, I136M–actin$_{EGFP}$ aggregates may represent non-polymerized actin in a conformation incompatible with DNase I binding.

To examine endogenous actin expression in transfected cells, cells were labeled with antibodies recognising anti-alpha skeletal actin (SKA-1) and anti-sarcomeric actin (5C5, cardiac and skeletal actin isoforms) antibodies. Double-labeling with anti-alpha skeletal actin (SKA-1) and anti-sarcomeric actin (5C5) weakly stained actin accumulations from I136M and R183G actin constructs, but not the V163L and V163M intranuclear aggregates (data not shown). These results suggest that aggregates formed by the different mutant actin constructs are not identical, and that antibody inaccessibility due to steric hindrance needs to be considered when interpreting co-labeling results.

To provide further evidence that the formation of actin aggregates represents inherent misfolding of mutant actin and is not a function of EGFP-fusion, we performed a control study using an untagged V163L–actin construct. The V163L mutation was selected, as virtually every myoblast transfected with the V163L–actin$_{EGFP}$ construct displays intranuclear actin aggregates, and these aggregates may be co-labeled by phalloidin. Analysis of C2C12 myoblasts transfected with an untagged V163L-actin construct clearly demonstrates

Figure 3. Western analysis of sarcomeric protein expression in nemaline myopathy. Immunoblot analysis of (**A**) mild and (**B**) severe *ACTA1* NM patients. Frozen muscle biopsy sections were fractionated into insoluble and soluble protein pools. Solublized lysates were separated by SDS–PAGE using 3–12% polyacrylamide gradient gels, and transferred to PVDF membranes. There is an increase in levels of gamma-filamin, alpha-actinin, myotilin and desmin in many NM patients. Nebulin expression is secondarily reduced in some NM patients with a primary abnormality in *ACTA1* [(3A) lane 6; (3B) lanes 2,5,6,9,10]. Control muscle specimens were histologically normal and obtained from individuals with no history of neuromuscular disease. y = years, wks = weeks. (A) Lane 1, control 1 (quadriceps, 28y); Lane 2, control 2 (quadriceps, 5y); Lane 3, patient G268C (unknown site, 5y); Lane 4, patient I136M (deltoid, 28y); Lane 5, patient N115S$_a$ (quadriceps, 17y); Lane 6, patient N115S$_b$ (quadriceps, 36y); Lane 7, patient TPM$_a$ (*TPM3* M9R mutation) (adductor pollicis, 46y); Lane 8, TPM$_b$ (deltoid, 46y); Lane 9, control 3 (deltoid, 38y). Patient N115S$_a$ is the daughter of patient N115S$_b$. TPM$_a$ and TPM$_b$ represent two separate muscle samples derived from the same patient at the time of autopsy. (B) Lanes 1 and 8, control 1 (psoas, 36/40 wks); Lane 2, NM1 (quadriceps, 36/40 wks); Lane 3, patient T66I$_a$ (vastus lateralis, 39/40 wks); Lane 4, patient T66I$_b$ (rectus abdominus, 10 wks); Lane 5, patient R183G (quadriceps, 7 wks); Lane 6, NM2 (deltoid, 8 wks); Lanes 7 and 11, control 2 (unknown site, 26 days); Lane 9, patient E72K (quadriceps, 35/40 wks); Lane 10, patient I357 (vastus lateralis, 5 wks). T66I$_a$ and T66I$_b$ represent two muscle samples from the same patient, obtained in separate biopsy operations at different ages.

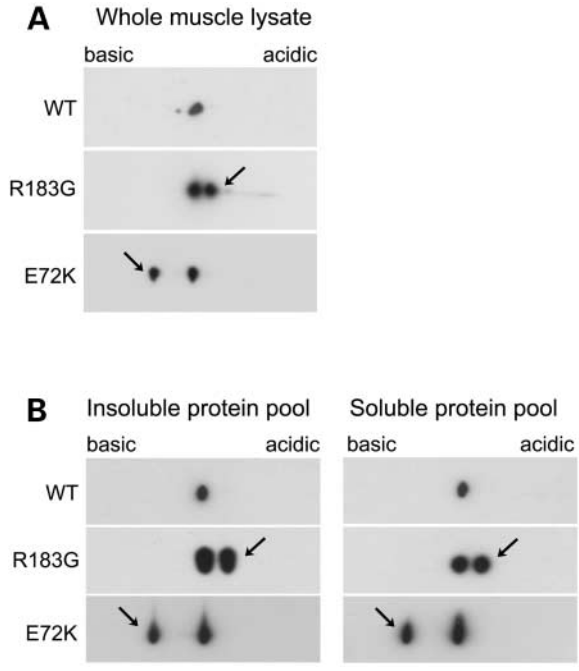

Figure 4. Isoelectric focusing of NM muscle samples supports the hypothesis of a dominant-negative 'poison-protein' effect. IEF of patients R183G and E72K from frozen muscle biopsies using (**A**) whole muscle lysates and (**B**) extraction of muscle into insoluble and soluble protein pools. The PVDF membranes were probed with an alpha-skeletal actin-specific antibody (SKA-1) (1:300 dilution). A single spot corresponding to wild-type (WT) alpha-skeletal actin is evident in the age-matched control sample (predicted p*I* of 5.23). In contrast, two spots are clearly evident for patients R183G and E72K. The R183G mutant actin (predicted p*I* of 5.16) is slightly more acidic and is expressed at roughly equal levels (R183G, arrowhead) to WT actin. E72K is more basic (predicted p*I* of 5.38) and is expressed at lower levels (E72K, arrowhead) compared with WT. Both mutant actin isoforms, R183G and E72K, localize to the insoluble protein pool in significant quantities, suggesting that they both contribute to the sarcomeric thin filaments, supporting a dominant-negative (poison-protein) effect rather than haploinsufficiency (shortage of normal actin protein).

intranuclear actin aggregates, identified through phalloidin staining (Fig. 5B,vi). No evidence of phalloidin-labeled intranuclear actin aggregates was observed using an untagged wild-type actin construct (data not shown). Additionally, we performed co-transfection studies combining V163L–actin$_{EGFP}$, together with WT actin fused to the red fluorescent protein DsRED (pDsRed2-N1, BD Biosciences Clontech), and showed that WT-actin$_{dsRED}$ did not localize to the actin aggregates (data not shown).

To determine that C-terminal EGFP tagging of α-skeletal actin did not impair its normal polymerization and incorporation into sarcomeric thin filaments, we differentiated myoblasts transfected with WT-actin$_{EGFP}$. Upon differentiation, striated staining for WT-actin$_{EGFP}$ was observed in a subset of myotubes, and demonstrates that actin$_{EGFP}$ conjugates can correctly localize within the sarcomeric thin filament (Fig. 5B,viii). The ability of mutant actin isoforms to contribute to the sarcomeric thin filament is now the subject of further studies within our laboratory.

Mutations in α-skeletal actin differentially affect polymerization and incorporation into actin filaments

We examined the ability of several actin isoforms to polymerize and incorporate into the filamentous cytoskeleton of transfected C2C12 myoblasts and differentiated myotubes. C2C12 myoblasts were transfected with C-terminal Flag-tagged mutant actin constructs (WT, I136M, V163L, R183G, C268G and I357L), trypsinized and re-plated onto feeder layers of confluent cartilage fibroblasts. Fibroblast feeder layers prolong the lifetime of spontaneously contracting cultured myotubes, permitting a greater degree of sarcomeric maturity (36). Duplicate wells were harvested 1 day after replating (D0) and after 3 (D3) and 6 days (D6) of differentiation. Typically, C2C12 cultures would be twitching on D3, and contracting more vigorously on D6, reflecting more advanced sarcomeric development at later differentiation time-points. Figure 6B shows relative levels of actin$_{FLAG}$ present in the insoluble and soluble protein pools at the three different time-points. The insoluble fraction is enriched for actin$_{FLAG}$ contained within large cytoskeletal and sarcomeric actin filaments, and will also include actin aggregates. The soluble protein pool contains soluble actin$_{FLAG}$ monomers, and short actin filaments not sedimented by centrifugation at 15 000*g*.

In undifferentiated myoblasts (D0), wild-type actin was present at roughly equal levels in soluble (48% total actin) and insoluble (52% total actin) fractions. As C2C12 myotubes differentiated, there was a concomitant increase in levels of insoluble actin, reaching 76% of total actin levels by D6 (Fig. 6).

I136M–actin$_{FLAG}$, G268C–actin$_{FLAG}$ and I357L–actin$_{FLAG}$ constructs behaved similarly to WT-actin$_{FLAG}$ (Fig. 6), with approximately half of the expressed actin detected within the insoluble cytoskeleton at D0, increasing to 69–76% by D6. In contrast, R183–actin$_{FLAG}$ contributed less efficiently to insoluble actin filaments, localizing predominantly to the soluble protein fraction (∼70% total actin) in undifferentiated myoblasts (D0) (H_0:$T \neq t$, $P \leq 0.001$) and early myotubes (D3) (H_0:$T \neq t$, $P \leq 0.001$), with gradual incorporation into insoluble actin filaments (53% total actin) in more mature myotubes (D6) (H_0:$T \neq t$, $P \leq 0.004$). These results suggest an impaired ability of R183-actin$_{FLAG}$ to contribute to long, insoluble actin filaments, either in conjunction with cytoplasmic actin isoforms that predominate in undifferentiated myoblasts, or with sarcomeric actin isoforms that predominate in differentiated myotubes (36, data not shown).

In contrast, V163L–actin$_{FLAG}$ exhibited near-maximal levels of insoluble actin at D0 (68% total actin) (H_0:$T \neq t$, $P \leq 0.024$), suggesting enhanced polymerization of V163L–actin$_{FLAG}$ with cytoplasmic actin isoforms expressed in undifferentiated myoblasts. However, levels of insoluble actin remained fairly constant with differentiation, and did not differ significantly from WT–actin$_{FLAG}$ at D3 or D6 (Fig. 6). A predisposition of V163L–actin$_{FLAG}$ for forming insoluble actin filaments is consistent with our immunocytochemical findings for V163L–actin$_{GFP}$, which forms filamentous intranuclear actin aggregates (Fig. 5). These results are also consistent with the pathology of patient V163L, who shows intranuclear rod bodies, and for whom large intracellular accumulations of filamentous actin were a striking feature.

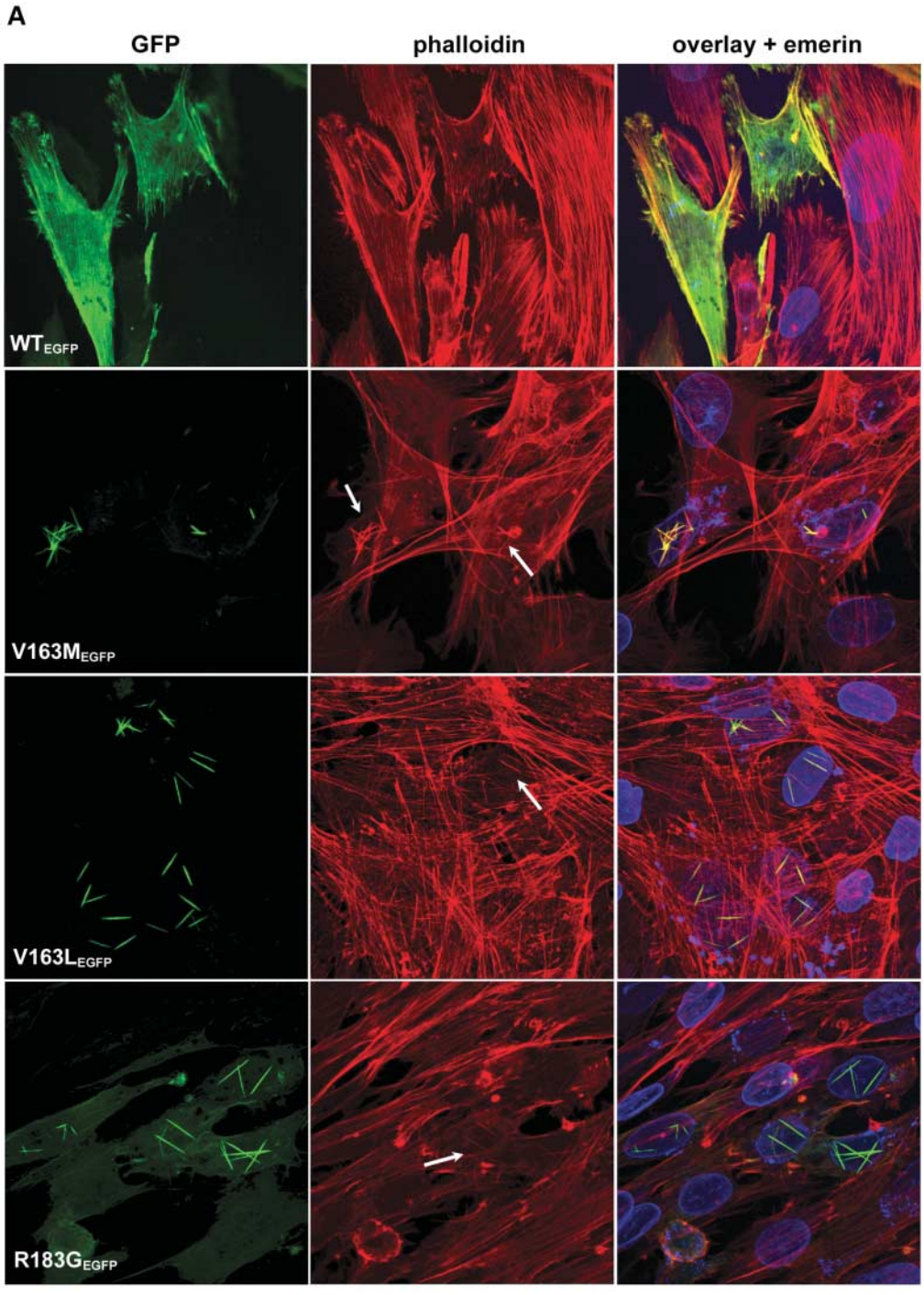

Figure 5. Nemaline myopathy actin mutants form abnormal aggregates in cultured C2C12 myoblasts. C2C12 myoblasts were transfected with EGFP-tagged actin constructs and stained with TRITC-phalloidin (red) and emerin (blue), labeled with a CY5-conjugated secondary antibody, to highlight cell nuclei. (**A**) EGFP fluorescence (left panel) shows diffuse cytoplasmic staining or stress-fibre staining for WT-actin$_{EGFP}$. In contrast, intranuclear rod-shaped aggregates were observed with V163M–actin$_{EGFP}$, V163L–actin$_{EGFP}$ and R183G–actin$_{EGFP}$ constructs. Note the very low levels of cytoplasmic staining with V163M–actin$_{EGFP}$ and V163L–actin$_{EGFP}$ constructs, compared with R183G–actin$_{EGFP}$ for which cytoplasmic and stress-fibre staining is clearly shown. Phalloidin co-labels actin aggregates formed by V163M–, V163L– and R183G–EGFP-tagged actin constructs [(A) middle panel, arrowheads]. (**B**) In addition to rod-shaped actin aggregates, star-like intranuclear aggregates were detected in a subset of cells transfected with V163L–actin$_{EGFP}$ (i) and V163M–actin$_{EGFP}$ (data not shown). (ii) Fragmentation of cytoskeletal actin filaments and cytoplasmic aggregates were a feature of a subset of cells transfected with R183G–actin$_{EGFP}$. (iii–v) I136M–actin$_{EGFP}$ produces cytoplasmic actin aggregates that do not label with phalloidin. (vi and vii) Intranuclear aggregates labelled by phalloidin are detected in C2C12 myoblasts transfected with untagged V163L–actin (arrowheads), demonstrating intranuclear actin aggregation is an inherent property of this actin mutation, and does not result from EGFP-tagging. (viii) Differentiation studies show that EGFP-tagged WT actin localizes normally to the sarcomeric thin filament. Confocal microscopy was performed using a Leica SP2 Scanning Laser Confocal Microscope using a 100× (HCX PL APO 1.40) oil lens with 1.84–3.5 zoom.

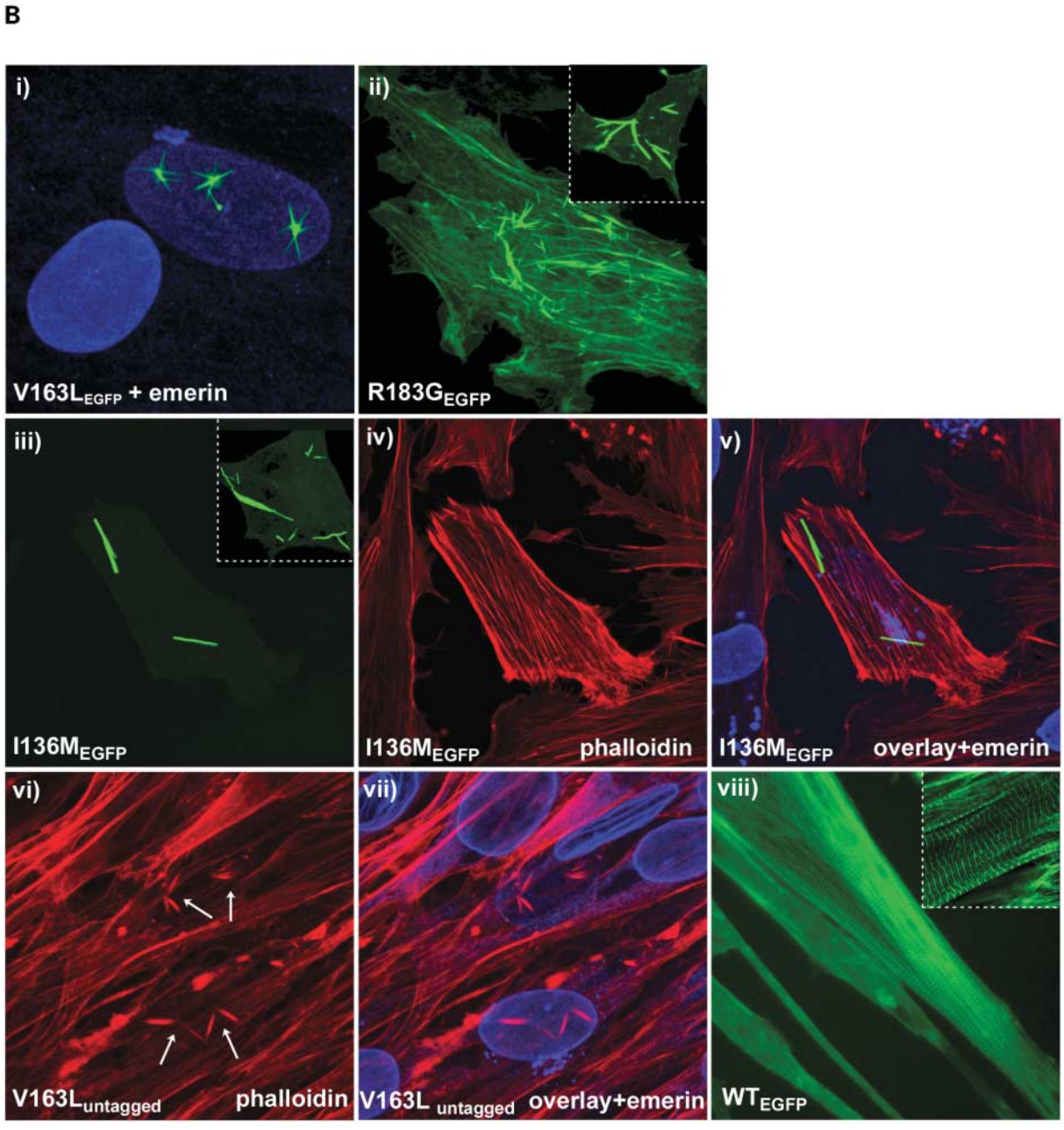

Figure 5. Continued.

A conservative amino acid substitution (I357L) within α-skeletal actin results in conformational changes detected by native PAGE

Thus far, all studies examining the properties of a mutant actin isoform found in one severely affected NM patient showed no significant differences to wild-type actin (patient I357L). The amino acid substitution in this patient is very conservative, isoleucine 357 to leucine, but results in a lethal phenotype. Molecular modeling of this mutation highlights potential alterations in hydrogen bonding at the extreme C-terminus of G-actin (Fig. 8). Therefore, native polyacrylamide electrophoresis was used to explore whether altered mobility of I357L–actin could be observed.

Expression constructs containing cDNA sequences for WT actin, I357L and R183G were generated (actin sequence only, no EGFP or FLAG tag). 3T3 fibroblasts were transfected, and soluble actin was derived using 'G-actin' buffer (see Materials and Methods). PVDF membranes probed with anti-sarcomeric actin demonstrate the slightly slower mobility of I357L–actin (Fig. 7). Although subtle, this slight retardation in the native mobility of I357L–actin was repeated

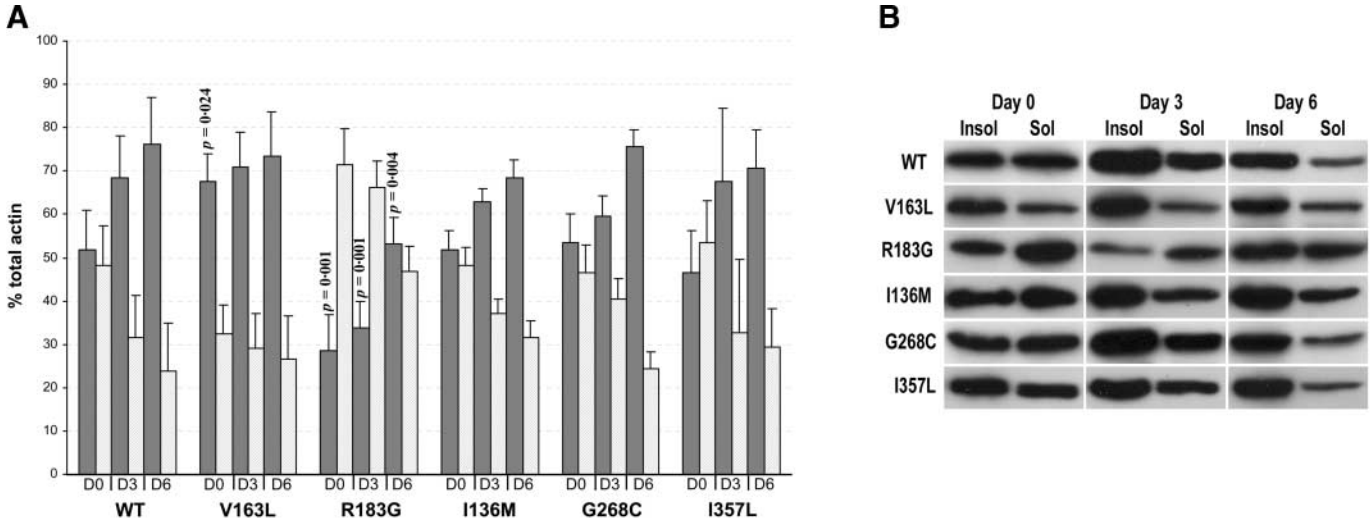

Figure 6. Mutations in α-skeletal actin differentially affect polymerization and incorporation into actin filaments in cultured C2C12 myotubes. C2C12 myoblasts transfected with FLAG-tagged actin constructs were harvested 24 h after replating (D0, myoblasts), and after 3 days (D3, immature myotubes) and 6 days (D6, more mature myotubes) of differentiation. Each sample was separated into insoluble (filled bars) and soluble (hatched bars) protein pools, using a buffer containing 0.5% Triton X-100. Solubilized lysates were separated by SDS–PAGE and transferred to PVDF membranes. Levels of $actin_{FLAG}$ contained within each protein pool was determined using an anti-FLAG antibody. Band intensity was quantified through densitometric analysis. The mean data from multiple experiments is shown in (**A**). WT, $n = 10$; V163L, $n = 4$; R183G, $n = 5$; I136M, $n = 4$; G268C, $n = 4$; I357L, $n = 6$. The comparison of means was performed using a Mann–Whitney non-parametric test. (**B**) Western analysis showing levels of $actin_{FLAG}$ within the insoluble (Insol) and soluble (Sol) protein pools. The results shown are data from a single experiment for each $actin_{FLAG}$ construct, at the three different time-points following transfection (D0, D3, D6).

on four separate occasions, and suggests a less compact three dimensional conformation of the actin monomer.

DISCUSSION

To date, 91 mutations in *ACTA1* have been identified in patients with NM and related disorders, including actinopathy and intranuclear rod myopathy. Our previous study has shown that the incidence of *ACTA1* mutations in idiopathic NM is roughly ∼20%, although the incidence of actin mutations within the subset of patients with severe-lethal congenital NM patients may be as high as 50% (5–7,13). This study examined a series of 10 NM patients with mutations in *ACTA1*, eight of whom have been described previously (5,6,13,33), and two new patients possessing novel *ACTA1* mutations (patients T661 and E72K).

The filamentous accumulations observed within the muscle fibers of patient V163M (Fig. 1I) are similar to the accumulations of filamentous actin previously described in three *ACTA1* NM patients (13,33). This may be a pathological feature common to patients with mutations in *ACTA1*, and may help direct mutational analysis (6). For patient E72K, muscle samples from three sites were examined at autopsy, although nemaline bodies were identified only in the quadriceps, not the psoas or diaphragm. This finding is supported by previous studies of NM patients in whom rods were not identified in some muscles (37–39) and highlights the importance of analysis of muscle samples from multiple sites for accurate diagnosis of NM.

Nebulin expression was markedly reduced in patient E72K, by immunostaining and western analysis (Figs 2 and 3B). Our laboratory has screened 23 idiopathic NM patients for nebulin expression, using a panel of five nebulin antibodies, and patient E72K exhibited the most striking abnormality observed to date (A. Domazetovska, unpublished data). Consequently, a defect in the nebulin gene was first considered as the potential disease candidate in this patient, and the identification of a primary mutation in *ACTA1* was a surprising but clinically important finding, with significant impact on genetic counseling for the patient's family. We have previously described nebulin abnormalities in two additional severe congenital *ACTA1* NM patients [R183G and I357L (5)]. These results show that protein analyses may not accurately guide mutation analysis and advocate screening of the *ACTA1* gene prior to pursuit of other disease candidates.

The reason for nebulin abnormalities in *ACTA1* NM patients is unclear, but is more common in severely affected patients and is more marked than observed abnormalities in other thin-filament proteins, such as tropomyosin. Although purely speculative, perhaps the low, absent or variable levels of nebulin within individual fibers of severely affected NM patients may reflect instability and increased turnover of the thin filament, whereby synthesis of the extremely large nebulin protein is unable to keep up with turnover.

Analysis of sarcomeric protein expression revealed that γ-filamin, α-actinin, myotilin and desmin are upregulated in many NM patients, compared with unaffected age-matched controls. This may be due to the association of these proteins with the Z-disc, and their localization within nemaline bodies. However, effects relating to changes in fiber-type, composition or from regeneration cannot be excluded. α-Actinin 2 and myotilin have been shown to be components of nemaline bodies (40–42). There is some evidence for desmin expression

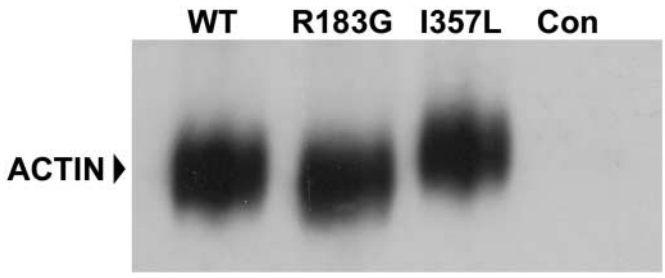

Figure 7. A conservative amino acid substitution (I357L) within alpha-skeletal actin results in conformational changes detected by native PAGE. NIH3T3 cells were transfected with untagged wild-type (WT) actin, and untagged mutant actin constructs R183G and I357L. Cells were harvested, extracted for soluble actin protein and separated by non-denaturing electrophoresis using a 5–12% gradient gel. The blot was probed with a sarcomeric actin-specific antibody (5C5, Sigma) and the bands shown are the only bands visible on the blot. Under these conditions, the I357L mutant actin protein runs slightly slower than WT actin. This subtle shift in mobility was repeated on four separate occasions, and suggests an altered tertiary conformation of this actin monomer. Control (Con) represents untransfected NIH3T3 cells.

within nemaline bodies (43,44), and we have observed positive staining for filamin within nemaline bodies of a subset of NM patients (unpublished data). Filamin showed variable localization to either the insoluble or soluble pool in control samples (Fig. 3B, compare lanes 1 and 7), although the significance of this finding is unknown. Studies have shown that filamin has dual localization both at the Z-line and at the subsarcolemmal cytoskeleton (20,21). Our results may reflect variation in tethering at these sites, and thus sensitivity to 0.5% Triton X-100.

IEF demonstrates that mutant actin isoforms, R183G and E72K, are present at significant levels within the skeletal muscle of the affected patient. We also demonstrate that the mutant actin isoforms contribute to the insoluble protein pool, comprising the insoluble cytoskeleton and sarcomeric apparatus. Because the majority of α-skeletal actin found in muscle comprises the sarcomeric thin filament, our results imply that a significant portion of the mutant actin isoform is present within the sarcomeric thin filament, suggesting a dominant-negative mode of disease pathogenesis. However, the mutant actin isoforms may also be contained in nemaline bodies or actin aggregates. For patients where large regions of their muscle fibers are occupied by nemaline bodies or filamentous aggregates of actin, we cannot exclude the possibility that a shortage of functionally normal actin able to contribute to sarcomeric thin filaments also contributes to disease pathogenesis.

The recent identification of a severe NM patient homozygous for a nonsense mutation in *ACTA1* (14), born to phenotypically normal consanguineous parents (N.G. Laing *et al.*, unpublished data), implies that possession of a single functional actin allele is sufficient for normal muscle function. A dominant-negative mode of disease pathogenesis in *ACTA1* NM is supported by studies in the KM88 (null mutation of the muscle-specific actin gene *Act88F*) *Drosophila* flightless mutant, expressing no sarcomeric actin within the flight muscle (45). *P*-element transformation of a panel of mutant actin isoforms demonstrated a clear gene-dosage effect that was mutation specific (17). Transformation of KM88 flies with WT actin restored almost normal flight ability. Expression of a panel of actin mutants as a 1:1 ratio with WT actin resulted in a gradient of effects, from moderate impairment in flight ability to a completely flightless phenotype. In some cases, a flighted phenotype could be restored, or partially restored, using a lower ratio of mutant : WT actin (1:2), but restoration of flight ability by this means was mutation-dependent, with maintenance of a flightless phenotype for a subset of more severe actin mutants (17).

Expression of EGFP-tagged mutant actin constructs in C2C12 myoblasts demonstrates abnormal aggregation of several mutant actin isoforms into 'rod-shaped' actin accumulations. Intranuclear accumulations resulted from transfection of V163L–actin$_{EGFP}$, V163M–actin$_{EGFP}$ and R183G–actin$_{EGFP}$ constructs. V163L–actin$_{EGFP}$ and V163M–actin$_{EGFP}$ constructs were modeled on patients with intranuclear rod myopathy, whereas R183G–actin$_{EGFP}$ is modeled on a patient whose biopsy showed no evidence of intranuclear rods, although this may reflect the limited sampling associated with EM analysis. Only cytoplasmic actin accumulations were evident with the I136M–actin$_{EGFP}$ construct. This observation is consistent with the pathology of the patient's muscle (patient I136M), which contains numerous nemaline bodies located exclusively within the cytoplasm (5). Other mutant actin$_{EGFP}$ constructs (T66I, E72K, N115S, G268C and I357L) did not induce actin accumulations in C2C12 myoblasts, and future experiments will now focus on the contribution of these mutant actin isoforms to the sarcomeric thin filament.

Actin has two NESs thought to govern the active transport of actin from the nucleus in into the cytoplasm mammalian cells (35). Disruption of conserved residues within the actin NES results in retention of actin within the nucleus (35). Molecular modeling shows the proximity of residues V163 and R183 to amino acids within the actin NES, located within the 4 Å maximal radius for bond formation. The intranuclear actin aggregates we observe in C2C12 myoblasts transfected with V163L–actin$_{EGFP}$, V163M–actin$_{EGFP}$ and R183G–actin$_{EGFP}$ constructs bear striking resemblance to intranuclear 'paracrystal structures' reported by Wada *et al.* (35), following treatment of murine fibroblasts with leptomycin B, a nuclear export inhibitor. Thus, our results suggest that NM mutations V163L, V163M and R183G may induce steric or conformational changes of the NES, perhaps affecting the binding of effector molecules to this region, contributing to the nuclear retention and aggregation of these mutant actin isoforms.

Our study employed the intracellular environment of differentiating C2C12 myoblasts to examine the ability of NM mutant actin isoforms to polymerize with endogenous actin isoforms, and contribute to the insoluble cytoskeleton and developing sarcomeric apparatus. R183G–actin$_{FLAG}$ showed a reduced ability to incorporate into insoluble actin filaments, compared with WT–actin$_{FLAG}$, producing high levels of soluble actin (actin monomers or short filaments not pelleted by 15 000*g*). These alterations in polymerization capacity were highly significant (Fig. 6A). The R183 amino acid residue lies near to the ATP-binding site of actin (Fig. 8). Alterations in ATP binding would likely affect actin polymerization, and several *ACTA1* NM mutations cluster to this region (6). Although R183 is not predicted

to form bonds with ATP directly, it does interact with two residues that are thought to mediate ATP-binding (S14 and D157) (46–48). Residue S14 has crucial role in ATP-binding, and mutation of this residue to glycine or cysteine results in a lethal phenotype in yeast (48). Polymerization of actin is a major ATP-consuming reaction, and depletion of intracellular ATP levels has been shown to produce cytoplasmic actin aggregates in cultured rat neurons (49,50). Thus, whether actin aggregates observed following transfection of V163L, V163M, R183G and I136M EGFP-tagged mutants relates to intracellular levels of ATP merits further investigation.

Alterations in polymerization of NM *ACTA1* mutants are complemented by a recent study showing increased levels of short-actin filaments (not pelleted by centrifugation at 400 000 *g*) following *in vitro* polymerization of skeletal actin purified from muscle from a NM *ACTA1* patient possessing a M132V missense mutation (51). Similarly, analysis of a large panel of NM *ACTA1* mutants found impaired polymerization of several mutant actin isoforms, using *in vitro* translation assays, and sedimentation with carrier actin (52). Moreover, the authors also demonstrate increased association of mutant actin isoforms with chaperone proteins, using *in vitro* binding assays, and also document abnormal aggregation of mutant actin protein products in non-muscle cells (52).

In contrast, V163L–actin$_{FLAG}$ exhibited maximal levels of insoluble actin filaments immediately following transfection, exceeding levels observed with WT–actin$_{FLAG}$. An enhanced capacity of V163L–actin$_{FLAG}$ to form insoluble actin species is supported by our immunohistochemical findings in V163L–actin$_{EGFP}$-transfected C2C12 myoblasts, where brightly fluorescent filamentous actin aggregates are the only discernible feature, with low or undetectable levels of cytoplasmic or stress-fibre staining. These findings also compare with the pathology of patient V163L, who shows intranuclear rod bodies, and for whom large intracellular accumulations of filamentous actin were a striking feature. Our molecular modeling shows that V163 lies within 4 Å of residues A170 and I175 of NES1. I175 is one of the four critical hydrophobic residues found in all NES sequences shown to be important for functional nuclear export (35). A170 lies outside the maximal 4 Å radius for bond formation following substitution of V163 for L163. Sparrow *et al.* (6) also note that substitution of leucine for valine at position 163 may result in distortion of the actin hinge region, thought to be important for ATP binding and exchange, and integral to actin filament formation and stability.

In summary, our studies provide a number of insights into the pathogenetic mechanisms of *ACTA1* NM. We provide, for the first time, direct evidence for a dominant-negative effect of mutant actin isoforms in NM. Our results show that mutant actin is present in patient skeletal muscle and is likely incorporated into the sarcomeric thin filament. *In vitro* studies demonstrate that formation of actin aggregates within the cytoplasm and nucleus, altered polymerization and abnormal folding are the properties of NM *ACTA1* mutants. Some of these effects are mutation-specific, reflecting involvement of different functional domains of the actin molecule, and likely resulting in variations in the severity of muscle weakness seen in individual patients. A combination of these effects contributes to the common pathological hallmarks of NM, namely intranuclear and cytoplasmic rod formation, accumulation of thin filaments and myofibrillar disorganization.

MATERIALS AND METHODS

Patients

This study examines a series of 10 NM patients with mutations in *ACTA1* (Table 1). Patients N115S$_a$, N115S$_b$, I136M, R183G, G268C and I357L have been described in an earlier report (5). Patient V163L, with actin accumulations and intranuclear myopathy has been described previously (13,33). Patient V163M, with almost exclusive intranuclear rod myopathy has also been briefly reported (6) and is reported here in more detail. Patients T66I and E72K represent two new patients with *ACTA1* mutations not previously described. For comparison, muscle tissue was also studied from a NM patient with a missense mutation in *TPM3* (M9R) (8), and from two severe-congenital NM patients (patients NM1 and NM2) in whom the primary disease-causing mutation is unknown (routine *ACTA1* screening did not identify a mutation). Control samples were from patients with no form of neuromuscular disease and with normal muscle histology. Patients TPM, E72K, control 1 (36/40 week, psoas muscle, Fig. 3B) and control 2 (26 days, unknown site, Fig. 3B) were obtained at autopsy. Control 2 (quadriceps, 5 year, Fig. 3A) was obtained from a leg amputee. The remaining muscle samples were obtained at biopsy.

Constructs

All molecular biology reagents were obtained from Roche, unless otherwise specified. Primers were generated by Life Technologies or SigmaGenosys. All actin constructs were generated in the pEGFP-N1 backbone (Clontech). WT–actin$_{EGFP}$ was generated through amplification of α-skeletal actin from skeletal muscle-specific cDNA (forward primer 5′gatctcgag atgtgcgacgaagacgag3′; reverse primer 5′gcagaattcggaagcatttg cggtggacg3′) introducing *XhoI* (5′) and *Eco* RI (3′) restriction sites. Polymerase chain reaction products were gel purified (JETquick Gel Extraction spin kit, Genomed), and subcloned into the *Xho*I and *Eco*RI sites of the pEGFP-N1. EGFP-tagged actin mutants were generated through site-directed mutagenesis (QuickChange® Site-Directed Mutagenesis kit, Stratagene). To generate FLAG-tagged constructs, the EGFP cDNA was excised from WT-actin$_{EGFP}$ with *Eco*RI and *Not*I and the FLAG sequence was replaced using two annealed oligos (5′aattctggactacaaggacgacgatgacaagtagc3′; 5′ggccg ctacttgtcatcgtcgtccttgtagtccag3′) to generate pActin$_{FLAG}$. Mutant actin cDNAs were excised from the actin–EGFP constructs, using *Xho* I (5′) and *Eco* RI (3′), and subcloned into the same sites of pActin$_{FLAG}$.

Cell culture

All tissue culture media and reagents were purchased from Invitrogen unless otherwise specified. The isolate of C2C12 myoblasts (P21) used in this study forms spontaneously

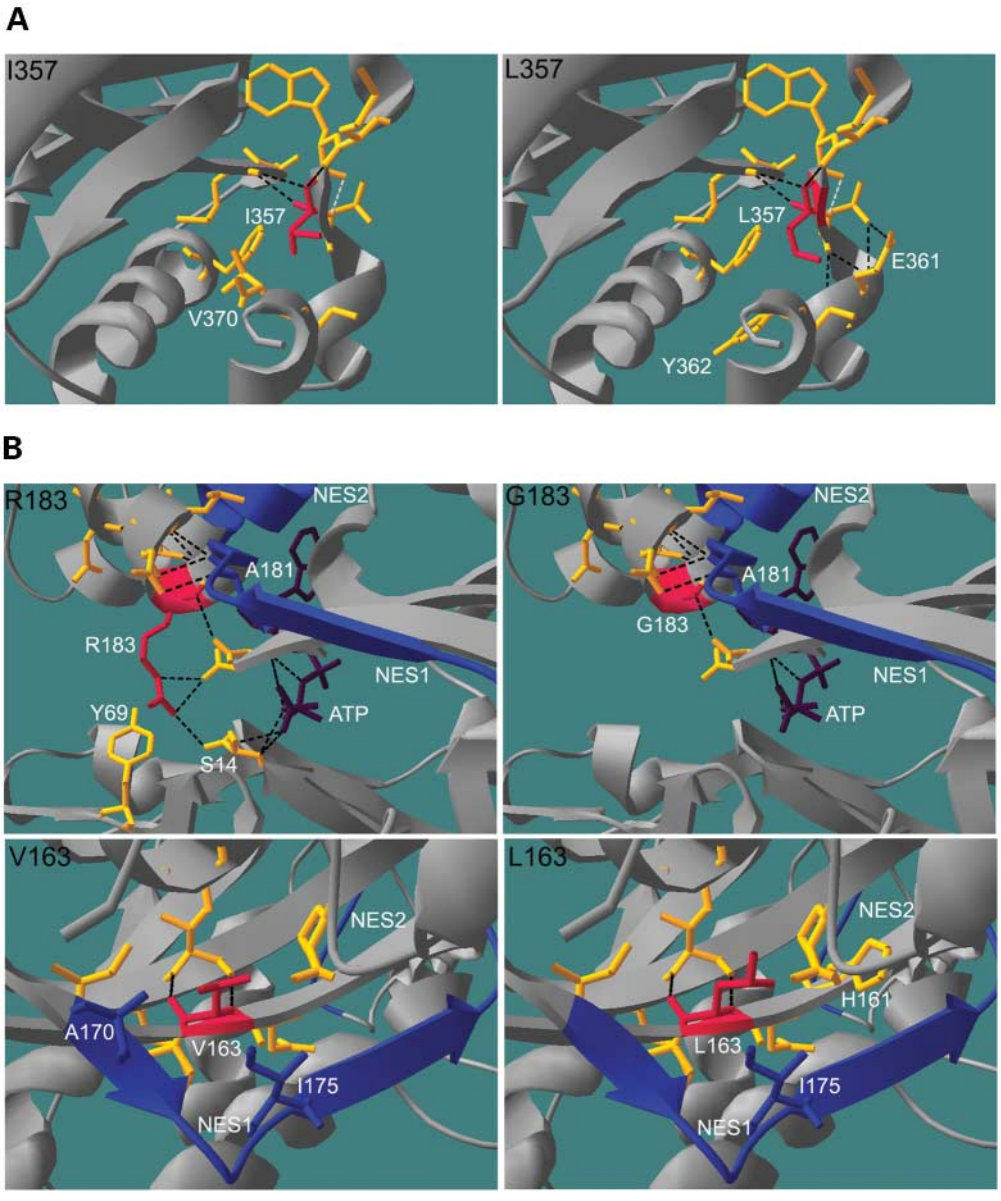

Figure 8. Molecular modeling of ACTA1 mutants I357L, R183G and V163L. (**A**) I357 resides at the C-terminus of actin (I357, red). Amino acid side chains within a 4 Å radius (the maximal distance for predicted bond formation) are shown in yellow. Predicted hydrogen bonding is shown as dashed lines (black, strong H-bonds; grey, weak H-bonds). Substitution of I357 to L357 (L357, red) predicts alterations in amino acid side chains within a 4 Å radius, and alterations in predicted hydrogen bonding within this C-terminal region. (**B**) Molecular modeling of actin residues R183 and V163 (R183 and V163, red) shows they are located near the nuclear export sequence 1 (NES1) of actin (35) (NES shown in blue). R183 lies within 4 Å of residue A181 located within NES1, and also resides adjacent to the ATP-binding site (ATP molecule shown in brown). Substitution of R183 to G183 (G183, red) alters the predicted amino acid side chains within a 4 Å radius and also alters predicted hydrogen bonding within the region. V163 lies within 4 Å of residues A170 and I175 of NES1. I175 is one of the four critical hydrophobic residues found in all NES sequences shown to be important for functional nuclear export (35). A170 lies outside the maximal 4 Å radius for bond formation following substitution of V163 for L163 (L163, red). Images were generated using DeepView/Swiss-Pdb Viewer (v3.7). http://www.expasy.org/spdbv/. The orientation of the L357, G183 and L163 substitutions were predicted by the Swiss-Pdb viewer software and are based on lowest predicted net energy.

contractile myotubes, and were a gift from Dr Edna Hardeman, Children's Medical Research Institute, Sydney. Cultures of neonatal human cartilage fibroblasts were provided by the Cytogenetics Department, Children's Hospital at Westmead, and de-identified in accordance with Children's Hospital at Westmead ethical guidelines. C2C12/fibroblast co-cultures were generated as described previously (36).

Transfections

C2C12 or NIH3T3 cells were trypsinized and plated 1 day prior to transfection, in growth media without antibiotics. The cells were transfected at 90% confluence using Lipofectamine2000^{TM}, according to the manufacturer's instructions. Briefly, per 2 cm^2 culture area, 1.2 μg of DNA and 3.6 μl

lipid were prepared in 0.1 ml of Optimem™ and incubated in 0.4 ml of growth media without antibiotics. Cells were transfected overnight, washed twice with phosphate buffered saline (PBS) and replenished with growth media. For polymerization studies, C2C12 cells were trypsinized after overnight transfection, and seeded in normal growth media onto confluent fibroblast monolayers prepared in 12-well plates. D0 cells were harvested the next day. The remaining cells were incubated in differentiation media, and D3 and D6 cells were harvested after 3 days and 6 days of differentiation, respectively.

Immunohistochemistry

Transfected C2C12 cells grown on thermonox coverslips (Nunc) were fixed and permeabilized in PBS containing 3% paraformaldehyde and 0.1% Triton-X 100 for 10–15 min at room temperature (RT). Samples were washed three times in PBS, then incubated in blocking buffer (PBS plus 2% bovine serum albumin) for 15 min at RT. Coverslips were incubated with a monoclonal antibody (mAb) that recognizes emerin (NCL-emerin, 1:100) (Novacastra Laboratories Ltd) diluted in blocking buffer for 1–2 h at RT. After washing, coverslips were blocked as mentioned earlier and then incubated with CY5-conjugated donkey anti-mouse IgG (1:200) (Jackson ImmunoResearch Laboratories. Inc.), together with TRITC–phalloidin (1:200) (Sigma) for 1 h at RT. Samples were washed three times in PBS and mounted on $22 \times 50\ mm^2$ glass coverslips using Fluorsave™ mounting reagent (Calbiochem). Confocal microscopy was performed using a Leica SP2 Scanning Laser Confocal Microscope. Autofluorescence of the thermanox coverslips was overcome by imaging through the glass coverslip. A droplet of oil was applied to the base of the thermanox coverslip and placed onto a glass slide (held in position by the oil), leaving the glass coverslip uppermost. All imaging was performed using sequential scanning, with restricted emission spectra shown to detect only the fluorophor of interest.

Antibodies

Antibodies used for western blotting; sarcomeric actin (5C5) (1:2000), sarcomeric tropomyosin (TM311) (1:30, 000), nebulin (NB2) (1:750) and anti-FLAG® M2 (1:5000) were obtained from Sigma. Anti-cardiac actin (1:1000) was purchased from American Research Products. mAbs that recognize desmin (NCL-DES) (1:500) and myotilin (NCL-MYOT) (1:2000) were purchased from Novacastra Laboratories Ltd. Troponin T_{slow} (CT3) (1:50), Troponin I_{fast} (MynT-fast) (1:400), and Troponin I_{slow} (MynT-slow) (1:1500) mAbs were obtained from the University of Iowa hybridoma bank. A polyclonal antibody (pAb) that recognizes α-actinin-2 (4B2) (1:60, 000) was kindly provided by Dr Alan Beggs (Harvard Medical School, Boston). The pAb filamin (FLN) (1:2500) was kindly provided by Prof Lou Kunkle (Harvard Medical School, Boston). A pAb that specifically recognizes α-skeletal actin (SKA1) (1:300) was made by Dr Sophie Clement (University of Geneva). Horse radish peroxidase-conjugated sheep anti-mouse (1:3000) and donkey anti-rabbit IgG (1:3000) antibodies were obtained from Amersham Biosciences.

Extraction of insoluble and soluble protein pools

Muscle samples. One 8 μm frozen muscle biopsy section, measuring roughly $10\ mm^2$, was suspended in 20 μl lysis buffer [LB; 50 mM MES pH 6.8, 1 mM EGTA pH 8.0, 50 mM KCl, 1 mM $MgCl_2$, 0.5% Triton X-100, (53)]. A protease inhibitor (PI) cocktail from Sigma was added immediately prior to use (1:500). Samples were incubated on ice for 15 min, then centrifuged at 15 000 *g* for 30 min at 4°C. The supernatant (soluble fraction) was removed and mixed with 4× SDS sample buffer [250 mM Tris pH 8.8, 8% SDS, 40% glycerol, 200 mM DTT, PI cocktail (1:125), bromophenol blue (BPB)]. The pellet (insoluble fraction) was resuspended in 1× SDS sample buffer [62.5 mM Tris pH 8.8, 6% SDS, 10% glycerol, 50 mM DTT, PI cocktail (1:500), BPB] and sonicated briefly. All samples were heat inactivated at 94°C for 4 min and stored at −20°C.

Cultured cells. Cultures were rinsed once with PBS and then incubated in 200 μl of LB for exactly 1 min. The LB was then transferred to an eppendorf containing 50 μl of 5× SDS-sample buffer [312.5 mM Tris pH 6.8, 10% SDS, 50% glycerol, 250 mM DTT, PI cocktail (1:500) and BPB] and represents the soluble protein pool. The cells were rinsed once with PBS, scraped into 200 μl of LB and then solubilized by the addition of 50 μl 5× SDS sample buffer. The insoluble protein fraction was briefly sonicated and both fractions were heat inactivated at 94°C for 4 min prior to storage at −20°C.

Western blot

Samples were thawed and heated to 94°C for 1 min immediately prior to loading on 3%–12% gradient SDS–PAGE gels. Western blot was performed as described (54).

Isoelectric focusing

Frozen muscle biopsy sections were separated into soluble and insoluble fractions as described earlier. The insoluble filaments were washed once in 1 ml of LB and re-centrifuged at 15 000 *g* for 10 min at 4°C. Both insoluble and soluble protein fractions were resuspended in rehydration solution [2% Triton-X 100, 8 M urea, 2% IPG buffer pH 4–7 (Amersham Biosciences), 36 mM DTT, PI cocktail (1:500), BPB], sonicated and solubilized for 20–30 min on ice. To determine equal loading of patient and control samples, 5 μl aliquots were separated by SDS–PAGE and western blotted for sarcomeric actin (5C5 Sigma antibody). Protein samples were used to hydrate 13 cm immobiline dry strips (pH 4–7, Amersham Biosciences) overnight at RT. The strips were focused using a Multiphor IEF unit (Amersham Biosciences) for a total of 21 000 V/h. Focused strips were incubated in SDS equilibration buffer (50 mM Tris–Cl pH 8.8, 6 M urea, 30% glycerol, 2% SDS, 10 mM DTT and BPB) with shaking for 15 min and separated in the second dimension using 9% acrylamide slab gels. The isoelectric point (p*I*) for proteins was calculated using the p*I* analysis tool available on the website http://www.expasy.org/.

Native gel electrophoresis

Transfected NIH3T3 fibroblasts (one 6-well) were scraped into PBS and pelleted at 300 *g* for 3 min. Residual PBS was aspirated, and the cell pellet was resuspended in 35 µl 'G-actin' buffer (2 mM Tris pH 8.0, 0.2 mM $CaCl_2$, 0.2 mM ATP, 0.5 mM phenyl methyl sulfonyl fluoride. The suspension was frozen on dry ice and thawed in the fingertips three times, taking care to 'just thaw' the samples. The samples were incubated in ice for 20 min and then spun at 15 000 *g* for 5 min at 4°C. The supernatant was transferred to a fresh tube, and combined with an equal volume of loading buffer (100 mM Tris pH 8.8, 20% glycerol, BPB). 10 µl aliquots were separated using a 5–12% non-denaturing gradient gel (375 mM Tris pH 8.8) in Tris–glycine electrophoresis buffer (25 mM Tris, 192 mM glycine, pH 8.3) with cooling to 16°C. Prior to transfer, the gel was incubated in tris–glycine buffer containing 0.1% SDS for 15 min with agitation. Proteins were then transferred to PVDF membrane using Towbin's transfer buffer (25 mM Tris, 192 mM glycine, 20% methanol, pH 8.3) at 35 V for 16 h, with recirculating water cooled to 16°C.

ACKNOWLEDGEMENTS

We would like to thank Dr Lesley C. Ades, Dr Susan Arbuckle and Dr Claire Cooke-Yarborough (Children's Hospital at Westmead, NSW, Australia), Dr Joseph Dezordi (Townsville Hospital, QLD, Australia), Dr Christine Oley (Royal Children's Hospital Brisbane, QLD, Australia) and Dr David Hutchinson (Auckland Hospital, New Zealand) for referral of patients and patient material. This work was funded by the National Health and Medical Research Council (NHMRC #139039) Australia (2001–2005). B.I. and A.D. are supported by Australian Postgraduate Award (APA) scholarships.

REFERENCES

1. Wallgren-Pettersson, C., Pelin, K., Hilpela, P., Donner, K., Porfirio, B., Graziano, C., Swoboda, K.J., Fardeau, M., Urtizberea, J.A., Muntoni, F. *et al.* (1999) Clinical and genetic heterogeneity in autosomal recessive nemaline myopathy. *Neuromuscul. Disord.*, **9**, 564–572.
2. Pelin, K., Hilpela, P., Donner, K., Sewry, C., Akkari, P.A., Wilton, S.D., Wattanasirichaigoon, D., Bang, M.L., Centner, T., Hanefeld, F. *et al.* (1999) Mutations in the nebulin gene associated with autosomal recessive nemaline myopathy. *Proc. Natl Acad. Sci. USA*, **96**, 2305–2310.
3. Sewry, C.A., Brown, S.C., Pelin, K., Jungbluth, H., Wallgren-Pettersson, C., Labeit, S., Manzur, A. and Muntoni, F. (2001) Abnormalities in the expression of nebulin in chromosome-2 linked nemaline myopathy. *Neuromuscul. Disord.*, **11**, 146–153.
4. Wallgren-Pettersson, C., Donner, K., Sewry, C., Bijlsma, E., Lammens, M., Bushby, K., Giovannucci, U.M., Lapi, E., Odent, S., Akcoren, Z. *et al.* (2002) Mutations in the nebulin gene can cause severe congenital nemaline myopathy. *Neuromuscul. Disord.*, **12**, 674–679.
5. Ilkovski, B., Cooper, S.T., Nowak, K., Ryan, M.M., Yang, N., Schnell, C., Durling, H.J., Roddick, L.G., Wilkinson, I., Kornberg, A.J. *et al.* (2001) Nemaline myopathy caused by mutations in the muscle alpha-skeletal-actin gene. *Am. J. Hum. Genet.*, **68**, 1333–1343.
6. Sparrow, J.C., Nowak, K.J., Durling, H.J., Beggs, A.H., Wallgren-Pettersson, C., Romero, N., Nonaka, I. and Laing, N.G. (2003) Muscle disease caused by mutations in the skeletal muscle alpha-actin gene (ACTA1). *Neuromuscul. Disord.* **13**, 519–531.
7. Agrawal, P.B., Strickland, C.D., Midgett, C., Morales, A., Newburger, D., Poulos, M.H., Tomczak, K.K., Ryan, M.M., Iannaccone, S.T., Crawford, T.O. *et al.* (2004) Heterogeneity of nemaline myopathy cases with skeletal muscle α-actin gene mutations. *Ann Neurol.*, **56**, 86–96.
8. Laing, N.G., Wilton, S.D., Akkari, P.A., Dorosz, S., Boundy, K., Kneebone, C., Blumbergs, P., White, S., Watkins, H., Love, D.R. *et al.* (1995) A mutation in the alpha tropomyosin gene *TPM3* associated with autosomal dominant nemaline myopathy *NEM1*. *Nat. Genet.*, **10**, 249–231.
9. Tan, P., Briner, J., Boltshauser, E., Davis, M.R., Wilton, S.D., North, K., Wallgren-Pettersson, C. and Laing, N.G. (1999) Homozygosity for a nonsense mutation in the alpha-tropomyosin slow gene *TPM3* in a patient with severe infantile nemaline myopathy. *Neuromuscul. Disord.*, **9**, 573–579.
10. Wattanasirichaigoon, D., Swoboda, K.J., Takada, F., Tong, H.Q., Lip, V., Iannaccone, S.T., Wallgren-Pettersson, C., Laing, N.G. and Beggs, A.H. (2002) Mutations in the slow muscle alpha-tropomyosin gene, *TPM3*, a rare cause of nemaline myopathy. *Neurology*, **59**, 613–617.
11. Donner, K., Ollikainen, M., Ridanpaa, M., Christen, H.J., Goebel, H.H., De Visser, M., Pelin, K. and Wallgren-Pettersson, C. (2002) Mutations in the beta-tropomyosin (*TPM2*) gene—a rare cause of nemaline myopathy. *Neuromuscul. Disord.*, **12**, 151–158.
12. Johnston, J.J., Kelley, R.I., Crawford, T.O., Morton, D.H., Agarwala, R., Koch, T., Schaffer, A.A., Francomano, C.A. and Biesecker, L.G. (2000) A novel nemaline myopathy in the Amish caused by a mutation in troponin T1. *Am. J. Hum. Genet.*, **67**, 814–821.
13. Nowak, K.J., Wattanasirichaigoon, D., Goebel, H.H., Wilce, M., Pelin, K., Donner, K., Jacob, R.L., Hubner, C., Oexle, K., Anderson, J.R. *et al.* (1999) Mutations in the skeletal muscle alpha-actin gene in patients with actin myopathy and nemaline myopathy. *Nat. Genet.*, **23**, 208–212.
14. Romero, N.B., Barois, A., Leroy, J.-P., Oddy, A., Durling, H., Fardeau, M. and Laing, N. (2003) Homozygous nonsence mutation of the *ACTA1* gene-clinical phenotype and muscle pathology. Abs. *Neuromuscul. Disord.*, **13**, 616.
15. Crawford, K., Flick, R., Close, L., Shelly, D., Paul, R., Bove, K., Kumar, A. and Lessard, J. (2002) Mice lacking skeletal muscle actin show reduced muscle strength and growth deficits and die during the neonatal period. *Mol. Cell. Biol.*, **22**, 5887–5896.
16. Okamoto, H., Hiromi, Y., Ishikawa, E., Yamada, T., Isoda, K., Maekawa, H. and Hotta, Y. (1986) Molecular characterisation of mutant actin genes which induce heat-shock proteins in *Drosophila* flight muscles. *EMBO J.*, **5**(3), 589–596.
17. Drummond, D.R., Hennessey, E.S. and Sparrow, J.C. (1991) Characterisation of missense mutations in the *Act88F* gene in *Drosophila melanogaster*. *Mol. Gen. Genet.*, **226**, 70–80.
18. Wertman, K.F., Drubin, D.G. and Botstein, D. (1992) Systematic mutational analysis of the yeast *ACT1* gene. *Genetics*, **132**, 337–350.
19. Sparrow, J.C., Drummond, D.R., Hennessey, E.S., Clayton, J.D. and Lindegaard, F.B. (1992) Drosophila actin mutants and the study of myofibrillar assembly. *Sympos. Soc. Expt. Biol.* **46**, 111–129.
20. Thompson, T.G., Chan, Y.M., Hack, A.A., Brosius, M., Rajala, M., Lidov, H.G., McNally, E.M., Watkins, S. and Kunkel, L.M. (2000) Filamin 2 (FLN2): a muscle-specific sarcoglycan interacting protein. *J. Cell Biol.*, **148**, 115–126.
21. van der Ven, P.F., Obermann, W.M., Lemke, B., Gautel, M., Weber, K. and Furst, D.O. (2000) Characterization of muscle filamin isoforms suggests a possible role of gamma-filamin/ABP-L in sarcomeric Z-disc formation. *Cell Motil. Cytoskeleton*, **45**, 149–162.
22. Maruyama, K. and Ebashi, S. (1965) Alpha-actinin, a new structural protein from striated muscle. II. Action on actin. *J. Biochem. (Tokyo)*, **58**, 13–19.
23. Blanchard, A., Ohanian, V. and Critchley, D. (1989) The structure and function of alpha-actinin. *J. Muscle Res. Cell Motil.*, **10**, 280–289.
24. Salmikangas, P., Mykkanen, O.M., Gronholm, M., Heiska, L., Kere, J. and Carpen, O. (1999) Myotilin, a novel sarcomeric protein with two Ig-like domains, is encoded by a candidate gene for limb-girdle muscular dystrophy. *Hum. Mol. Genet.*, **8**, 1329–1336.
25. Pollock, M. and Atkinson, B.G. (1985) The intermediate filament protein desmin in cardiac and skeletal muscle from normal and dystrophic (BIO 14.6) hamsters. *Can. J. Biochem. Cell Biol.*, **63**, 430–438.
26. Kashiwada, K., Nishida, W., Hayashi, K., Ozawa, K., Yamanaka, Y., Saga, H., Yamashita, T., Tohyama, M., Shimada, S., Sato, K. and Sobue, K. (1997) Coordinate expression of alpha-tropomyosin and caldesmon isoforms in association with phenotypic modulation of smooth muscle cells. *J Biol. Chem.*, **272**, 15396–15404.

27. Ruiz-Opazo, N. and Nadal-Ginard, B. (1987) Alpha-tropomyosin gene organization. Alternative splicing of duplicated isotype-specific exons accounts for the production of smooth and striated muscle isoforms. *J. Biol. Chem.*, **262**, 4755–4765.
28. Goodwin, L.O., Lees-Miller, J.P., Leonard, M.A., Cheley, S.B. and Helfman, D.M. (1991) Four fibroblast tropomyosin isoforms are expressed from the rat alpha-tropomyosin gene via alternative RNA splicing and the use of two promoters. *J. Biol. Chem.*, **266**, 8408–8415.
29. Perry, S.V. (2001) Vertebrate tropomyosin: distribution, properties and function. *J. Muscle Res. Cell Motil.*, **22**, 5–49.
30. Corbett, M.A., Akkari, P.A., Domazetovska, A., Cooper, S.T., North, K.N., Laing, N.G., Gunning, P.W. and Hardeman, E.C. A mutation in α-tropomyosin$_{slow}$ alters tropomyosin dimer preference in nemaline myopathy. *Ann. Neurol*., in press.
31. Donner, K., Pelin, K., Sandbacka, M., Ahola, H.V., Lehtokari, L. and Wallgren-Pettersson, C. (2003) Characterisation of nebulin isoforms in different types of skeletal muscle. *Abst. Neuromuscul. Disord.*, **13**, 616.
32. Clement, S., Chaponnier, C. and Gabbiani, G. (1999) A subpopulation of cardiomyocytes expressing alpha-skeletal actin is identified by a specific polyclonal antibody. *Circ. Res.*, **85**, e51–e58.
33. Goebel, H.H., Anderson, J.R., Hubner, C., Oexle, K. and Warlo, I. (1997) Congenital myopathy with excess of thin myofilaments. *Neuromuscul. Disord.*, **7**, 160–168.
34. Weeks, D.A., Nixon, R.R., Kaimaktchiev, V. and Mierau, G.W. (2003) Intranuclear rod myopathy, a rare and morphologically striking variant of nemaline rod myopathy. *Ultrastruct. Pathol.*, **27**, 151–154.
35. Wada, A., Fukuda, M., Mishima, M. and Nishida, E. (1998) Nuclear export of actin: a novel mechanism regulating the subcellular localization of a major cytoskeletal protein. *EMBO J.*, **17**, 1635–1641.
36. Cooper, S.T., Maxwell, A.L., Ghoddusi, M., Hardeman, E.C., Alexander, I.E., Allen, D.G. and North, K.N. (2004) C2C12 co-culture on a fibroblast substratum enables sustained survival of contractile, highly differentiated myotubes with peripheral nuclei and adult fast myosin expression. *Cell Motil. Cytoskeleton.*, **58**, 200–11.
37. Shafiq, S.A., Dubowitz, V., Peterson, H.D. and Milhorat, A.T. (1967) Nemaline myopathy: report of a fatal case, with histochemical and electron microscopic studies. *Brain*, **90**, 817–828.
38. Dubowitz, V. (1985) *Muscle Biopsy: A Practical Approach.* Balliere Tindall, London.
39. Ryan, M.M., Ilkovski, B., Strickland, C.D., Schnell, C., Sanoudou, D., Midgett, C., Houston, R., Muirhead, D., Dennett, X., Shield, L.K. *et al.* (2003) Clinical course correlates poorly with muscle pathology in nemaline myopathy. *Neurology*, **60**, 665–673.
40. Jockusch, B.M., Veldman, H., Griffiths, G.W., van Oost, B.A. and Jennekens, F.G. (1980) Immunofluorescence microscopy of a myopathy. α-Actinin is a major constituent of nemaline rods. *Expt. Cell Res.*, **127**, 409–420.
41. Wallgren-Pettersson, C., Jasani, B., Newman, G.R., Morris, G.E., Jones, S., Singhrao, S., Clarke, A., Virtanen, I., Holmberg, C. and Rapola, J. (1995) Alpha-actinin in nemaline bodies in congenital nemaline myopathy: immunological confirmation by light and electron microscopy. *Neuromuscul. Disord.*, **5**, 93–104.
42. Schroder, R., Reimann, J., Salmikangas, P., Clemen, C.S., Hayashi, Y.K., Nonaka, I., Arahata, K. and Carpen, O. (2003) Beyond LGMD1A: myotilin is a component of central core lesions and nemaline rods. *Neuromuscul. Disord.*, **13**, 451–455.
43. Muller-Hocker, J., Schafer, S., Mendel, B., Lochmuller, H. and Pongratz, D. (2000) Nemaline cardiomyopathy in a young adult: an ultraimmunohistochemical study and review of the literature. *Ultrastruct. Pathol.*, **24**, 407–416.
44. van der Ven, P.F., Jap, P.H., ter Laak, H.J., Nonaka, I., Barth, P.G., Sengers, R.C., Stadhouders, A.M. and Ramaekers, F.C. (1995) Immunophenotyping of congenital myopathies: disorganization of sarcomeric, cytoskeletal and extracellular matrix proteins. *J Neurol. Sci.*, **129**, 199–213.
45. Hiromi, Y. and. Hotta, Y. (1985) Actin gene mutations in *Drosophila*: heat shock activation in the indirect flight muscles. *EMBO J.*, **4**, 1681–1687.
46. Kabsch, W., Mannherz, H.G., Suck, D., Pai, E.F. and Holmes, K.C. (1990) Atomic structure of the actin: DNase I complex *Nature*, **347**, 37–44 [see comments].
47. Chen, X. and Rubenstein, P.A. (1995) A mutation in an ATP-binding loop of *Saccharomyces cerevisiae* actin (S14A) causes a temperature-sensitive phenotype *in vivo* and *in vitro*. *J. Biol. Chem.*, **270**, 11 406–11 414.
48. Schuler, H., Korenbaum, E., Schutt, C.E., Lindberg, U. and Karlsson, R. (1999) Mutational analysis of the Ser14 and Asp157 in the nucleotide-binding site of beta-actin. *Eur. J. Biochem.*, **265**, 210–220.
49. Minamide, L.S., Striegl, A.M., Boyle, J.A., Meberg, P.J. and Bamburg, J.R. (2000) Neurodegenerative stimuli induce persistent ADF/cofilin-actin rods that disrupt distal neurite function. *Nat. Cell Biol.*, **2**, 628–636.
50. Bamburg, J.R. and Wiggan, O.P. (2002) ADF/cofilin and actin dynamics in disease. *Trends Cell Biol.*, **12**, 598–605.
51. Marston, S., Mirza, M., Abdulrazzak, H. and Sewry, C. (2004) Functional characterisation of a mutant actin (Met132Val) from a patient with nemaline myopathy. *Neuromuscul. Disord.*, **14**, 167–174.
52. Costa, C.F., Rommelaere, H., Waterschoot, D., Sethi, K.K., Nowak, K.J., Laing, N.G., Ampe, C. and Machesky, L.M. (2004) Myopathy mutations in α-skeletal muscle actin causes a variety of molecular defects. *J. Cell Sci.*, in press.
53. Lyubimova, A., Bershadsky, A.D. and Ben Ze'ev, A. (1999) Autoregulation of actin synthesis requires the 3′-UTR of actin mRNA and protects cells from actin overproduction. *J. Cell Biochem.*, **76**, 1–12.
54. Cooper, S.T., Lo, H.P. and North, K.N. (2003) Single section western blot: improving the molecular diagnosis of the muscular dystrophies. *Neurology*, **61**, 93–97.